Synthesis of 1,1-Diisopropyl- or -Diphenyl -2,5-dibromo- or -bis (trimethylsilyl)-3,4-diphenyl-siloles and the Electrochemical Properties as Anode Materials for Lithium-Ion Battery

Yoon-ho Cho,[†] Young Min Jung,[‡] and Young Tae Park[†,*]

[†]*Department of Chemistry, Keimyung University, Daegu 42601, Korea. *E-mail: ytpark@kmu.ac.kr*
[‡]*Division of Green Energy Research, Daegu Gyeongbuk Institute of Science & Technology, Daegu 42988, Korea*

Received October 10, 2020, Accepted December 14, 2020, Published online December 27, 2020

Intramolecular cyclization of 1,1-diisopropyl- or diphenyl-bis(phenylethynyl)-silanes (**2a** and **2b**) followed by bromination or trimethylsilylation were carried out to yield 1,1-diisopropyl- or -diphenyl-3,4-diphenyl-2,5-dibromo-siloles (**3a** and **3b**) and 1,1-diisoproyl- or -diphenyl-3,4-diphenyl-2,5-bis(trimethylsilyl)-siloles (**4a** and **4b**), respectively. The structures of **3a**,**b** and **4a,b** were confirmed using ^{1}H, ^{13}C, and ^{29}Si NMR as well as FTIR spectroscopy. The absorption bands of the siloles **3a**,**b** and **4a,b** in THF were measured at 303–325 nm with the molar absorptivities of $1.85 \times 10^{3} \sim 2.18 \times 10^{3}$ cm^{-1}·M^{-1}. The excitation bands were measured at 347–376 nm and the emission peaks were measured at 409–445 nm. Cyclic voltammograms of **3a** and **3b** indicated oxidation peaks at 0.90 and 0.80 V and reduction peaks at −1.20 and −1.20 V, respectively. The cyclic voltammograms of **4a** and **4b** indicated two oxidation peaks between −0.05 and −0.95 V and two reduction peaks between −0.10 and −0.93 V, respectively. Compound **4a** exhibits a better long cycle performance by almost 1000 cycles as compared that of **3a** and **4b**. The rate performance test of the anodes **Li-3a** and **Li-4a** exhibited better performance properties at various C rate than Li-**4b**. According to discharge–charge curves, **4a** shows one plateau at approximately 0.58 V of the first discharge curve and the initial discharge specific capacity of 972 mAh/g. The electrochemical impedance spectroscopy of **4a** indicates low charge transfer resistance, good conductivity of the electrolyte, and fast chemical adsorption/desorption rate of electrolyte ions on electrode surface, due to the electronic structure of **4a**.

Keywords: 1,1-Diisopropyl-2,5-dibromo-Silole, 1,1-Diisopropyl-2,5-bis(trimethylsilyl)-Silole, 1,1-Diphenyl-2,5-dibromo-Silole, 1,1-Diphenyl-2,5-bis(trimethylsilyl)-Silole, Electrochemical properties, Lithium-ion battery

Introduction

Silole derivatives that are 1-silacyclic 5-membered compounds such as 1-silacyclopenta-2,4-dienes,[1] possess a lower π-electronic LUMO energy as compared to that of the corresponding cyclopentadiene.[2] This feature is attributed to the orbital interactions between butadiene π* and silylene σ*.[3] Silole-bearing compounds with π-conjugated skeletons have been extensively studied as photoluminescent[4–9] and electronic OLED materials.[10–15] 2,5-Silole dendrimers that are end-capped with phenyl-ethenyl-carbosilanes exhibit green or greenish-blue fluorescence.[16]

We have previously outlined the syntheses of silole-containing polymeric materials, for example, poly(1,1-disubstituted-3,4-diphenyl-2,5-silole)s and poly[(1,1-dihexyl-3,4-diphenyl-2,5-silolene)-*co*-(disubstitutedsilyl-ene or -germylene)]s.[9,17] We were also the first to repot the electrochemical properties such as cyclic voltammograms and the long cycling performances of 1,1-diethyl or -dihexyl-2,5-bis(trimethylsilyl)-3,4-diphenyl-siloles as active anode materials for lithium secondary battery.[18]

Herein, we report the synthesis and detailed electrochemical properties of 1,1-diisopropyl or -diphenyl-2,5-dibromo or -bis(tri-methylsilyl)-3,4-diphenyl-siloles (**3a, 3b, 4a**, and **4b**) as active anode materials for lithium secondary battery.

Experimental

General. All the solvents were purified before use according to a previously reported procedure.[19] ^{1}H and ^{13}C NMR spectra of the synthesized compounds were recorded in $CDCl_3$ using a JEOL 500 MHz FT-NMR spectrometer. The chemical shifts of the NMR spectra were measured using the residual proton signal of $CDCl_3$ or tetramethylsilane as an internal standard. Infra-red (IR) spectra were recorded using a Thermo Scientific FT-IR iD50 spectrophotometer. We obtained the UV–Vis absorption spectra using a Hewlett Packard 8453 spectrophotometer. The excitation and emission spectra were recorded using a Horiba Fluorolog-3-11 fluorescence spectrophotometer. We performed the cyclic voltammetry experiments with a Bio-

Logic Science Instruments model VSP potentiostat using a three-electrode cell system composed of an Ag/AgCl reference electrode, platinum wire counter electrode, and copper working electrode, wherein the potential window was between +2 and −2 V. We prepared a working electrode system by dipping a copper electrode in a hexane solution of the synthesized silole derivatives and then evaporating the solvent in a dry oven. The morphologies and surface analysis of the battery cell anodes were examined by field emission scanning electron microscopy with SEM Hitachi S-4800 (Ibaraki, Japan). The cell properties of the charge/discharge experiments were performed using a multichannel potentiostat/galvanostat of WonATech WMPG-1000. Electrochemical impedance spectroscopy was performed using a VersaSTAT 3 Model 500 Potentiostat Galvanostat of AMETEK Scientific Instrument (Kingston, UK) with VersaStudio 2.60.0 Software of Princeton Applied Research (New Jersey, USA).

Diisopropyldi(phenylethynyl)silane (2a) was prepared by the reaction of dichlorodiisopropylsilane (**1a**) with phenylacetylene that was treated with *n*-butyllithium following the procedure reported in the literature.[11,17,20] A yellowish viscous liquid of the product **2a** (33.6 g, 99.0%) was obtained. ^{1}H NMR (500 MHz, $CDCl_3$): δ 1.24 (m, $2CH(CH_3)_2$, 14H), 7.35 (m, 6H), 7.56 (m, 4H). ^{13}C NMR (125 MHz, $CDCl_3$): δ 12.478, 17.718, 87.559, 107.073, 122.834, 128.727, 132.192. ^{29}Si NMR (99 MHz, $CDCl_3$): δ −23.139. IR (neat) ν_{max}: 3057 ($\nu_{arC\text{-}H}$), 2954, 2865 (ν_{alC-H}), 2157 ($\nu_{C\equiv C}$), 1595, 1573, 1487, 1460, 1442 ($\nu_{arC=C}$), 831, 754, 725, 686 (ν_{Si-C}) cm^{-1}.

Diphenyldi(phenylethynyl)silane (2b) was prepared by the reaction of dichlorodiphenylsilane (**1b**) with phenylacetylene that was treated with *n*-butyllithium by means of the literature.[11,17,20] A yellowish viscous liquid of the product **2b** (29.3 g, 97.0%) was obtained. ^{1}H NMR (500 MHz, $CDCl_3$): δ 7.38 (m, 6H), 7.48 (m, 6H), 7.63 (m, 4H), 7.92 (m, 4H). ^{13}C NMR (125 MHz, $CDCl_3$): δ 87.733, 108.917, 122.519, 128.249, 128.403, 129.372, 130.418, 132.492, 133.125, 135.064. ^{29}Si NMR (99 MHz, $CDCl_3$): δ −48.02. IR (neat) ν_{max}: 3068, 3019(ν_{arC-H}), 2157($\nu_{C\equiv C}$), 1487, 1441, 1429($\nu_{arC=C}$), 881, 834, 752, 741, 688(ν_{Si-C}) cm^{-1}.

2,5-Dibromo-1,1-diisopropyl-3,4-diphenyl-silole (3a) was prepared by the intramolecular reductive cyclization of compound **2a**, followed by bromination as per previous literature.[11,17,20] A white powder of the product **3a** (4.38 g, 58.23%) was obtained. ^{1}H NMR (500 MHz, $CDCl_3$): δ 1.26(d, 12H, J = 7.4 Hz), 1.52(m, 2H), 6.94(m, 4H), 7.15 (m, 6H). ^{13}C NMR (125 MHz, $CDCl_3$): δ 9.800, 17.171, 119.772, 127.345, 127.547, 128.958, 137.289, 157.869. ^{29}Si NMR (99 MHz, $CDCl_3$): δ 7.463. IR (neat)) ν_{max}: 3056, 3018(ν_{arC-H}), 2952, 2864(ν_{alC-H}), 1488, 1459, 1441 ($\nu_{arC=C}$), 1075, 1022($\nu_{C\text{-}Br}$), 766, 694, 672, 642(ν_{Si-C}) cm^{-1}. UV–Vis (THF) λ_{max}, nm (ε, cm^{-1} M^{-1}): 325 (1.91×10^3).

2,5-Dibromo-1,1,3,4-tetraphenyl-silole (3b) was prepared by the intramolecular reductive cyclization of compound **2b** and subsequent bromination following previous literature.[11,17,20] A white powder of the product **3b** (4.18 g, 59.13%) was obtained. ^{1}H NMR (500 MHz, $CDCl_3$): δ 7.02(m, 4H), 7.18(m, 6H), 7.53(m, 6H), 7.86(m, 4H), ^{13}C NMR (125 MHz, $CDCl_3$): δ 120.041, 127.595, 127.624, 127.969, 128.507, 129.025, 131.194, 135.782, 136.896, 158.215. ^{29}Si NMR (99 MHz, $CDCl_3$): δ −16.49. IR (neat) ν_{max}: 3051(ν_{arC-H}), 1487, 1472, 1426($\nu_{arC=C}$), 1076, 1057, 1024($\nu_{C\text{-}Br}$), 769, 737, 717, 695(ν_{Si-C}) cm^{-1}. UV–Vis (THF) λ_{max}, nm (ε, cm^{-1} M^{-1}): 333 (2.18×10^3).

1,1-Diisopropyl-2,5-bis(trimethylsilyl)-3,4-diphenyl-silole (4a) was synthesized by the intramolecular reductive cyclization of compound **3a** and subsequent trimethylsilation according to previous reports.[11,17,20] A white powder of the product **4a** (3.57 g, 48.8%) was obtained. ^{1}H NMR (500 MHz, $CDCl_3$): δ −0.17(s, 18H), 1.15(d, 12H, J = 7.4 Hz), 1.44(m, 2H), 6.79(m, 4H), 7.01 (m, 6H). ^{13}C NMR (125 MHz, $CDCl_3$): δ 1.181, 11.884, 18.421, 125.897, 126.934, 129.190, 140.842, 143.453, 171.933. ^{29}Si NMR (99 MHz, $CDCl_3$): δ −9.92, 35.60. IR (neat) ν_{max}: 3059(ν_{arC-H}), 2947, 2863(ν_{alC-H}), 1458 ($\nu_{arC=C}$), 831, 776, 758, 698(ν_{Si-C}) cm^{-1}. UV–Vis (THF) λ_{max}, nm (ε, cm^{-1} M^{-1}): 303 (1.85×10^3).

1,1,3,4-tetraphenyl-2,5-bis(trimethylsilyl)-silole (4b) was synthesized by the intramolecular reductive cyclization of compound **3b**, followed by trimethylsilation according to previous literature.[11,17,20] A pale yellowish powder of the product **4b** (3.51 g, 41.9%) was obtained. ^{1}H NMR (500 MHz, $CDCl_3$): δ 0.00(s, 18H), 7.34(m, 4H), 7.47(m, 6H), 7.86(m, 6H), 8.23(m, 4H). ^{13}C NMR (125 MHz, $CDCl_3$): δ 0.700, 126.184, 126.990, 127.931, 128.756, 129.726, 132.634, 135.667, 142.607, 143.663, 171.662. ^{29}Si NMR (99 MHz, $CDCl_3$): δ −8.86, 8.41. IR (neat)) ν_{max}: 3066(ν_{arC-H}), 2964, 2892(ν_{alC-H}), 1470, 1428 ($\nu_{arC=C}$), 1242(ν_{C-C}), 833, 778, 759, 737, 697 (ν_{Si-C}) cm^{-1}. UV–Vis (THF) λ_{max}, nm (ε, cm^{-1} M^{-1}): 311 (2.12×10^3).

Fabrication of the anode materials for lithium-ion batteries. The active materials **3a**, **4a**, or **4b** were mixed with Super P and polyvinylidenefluoride (PVDF) in a ratio of 30:60:10 (wt %). Following this, the mixtures were stirred using zirconia ball-milling with *N*-methylpyrrolidone (NMP) as the solvent for 24 h. The well-mixed electrode material solution was coated onto a Cu foil current collector, using a doctor blade. The coated active material was then vacuum-dried at 50 °C and the temperature was gradually increased to 110 °C for 12 h to remove the NMP solvent. The cell assembly of the 2032 type coin cell for the electrochemical properties experiment was carried out inside a glove box filled with Ar gas. Batteries were fabricated into half cells, and the prepared active materials were used as working electrodes with a thickness of 10 μm. Lithium metal was used as the counter electrode and polypropylene (PP) was used as the separator. The electrolyte was

made of 1 M $LiPF_6$ in ethylene carbonate (EC) and dimethyl carbonate (DMC) at a 30:70 (vol %) ratio.

Results and Discussion

Synthesis. Scheme 1 shows the synthesis of the siloles **3a**, **3b, 4a**, and **4b** via reaction procedures that have been reported previously.[11,17,20] First, dichloro-diisopropyl- and -diphenyl-silanes (**1a** and **1b**) were treated with lithium phenylacetylide, *in situ* prepared in THF solution by the reaction of phenylacetylene with *n*-BuLi, affording diisopropyl- and diphenyl-bis(phenylethynyl)-silane (**2a** and **2b**). Then, intramolecular reductive cyclization reactions of **2a** and **2b** were carried out successively using lithium naphthalenide, anhydrous zinc chloride, and *N*-bromosuccinimide (NBS) to obtain the compounds **3a** and 3**b**, or using lithium naphthalenide, and chlorotrimethylsilane to yield **4a** and **4b**, respectively, in reasonably high yields.

We confirmed the structures of **3a**,**b** and **4a**,**b** through ^{1}H, ^{13}C, and ^{29}Si NMR as well as FTIR studies. Selected characteristics of the compounds have been summarized in Table 1.[21–24] Notably, the silicon peaks in the ^{29}Si NMR spectra of **3a** and **3b** were observed at 7.46 and −16.49 ppm, respectively, while the silicon peaks of **4a** and **4b** attached to the silole ring were observed at 35.60 and −8.86 ppm, respectively.[23] The spectral data indicate that the siloles **3a,b** and **4a,b** were successfully prepared through the intramolecular reductive cyclizations of the bis(phenylethynyl)silane **2a** and **2b**, respectively.

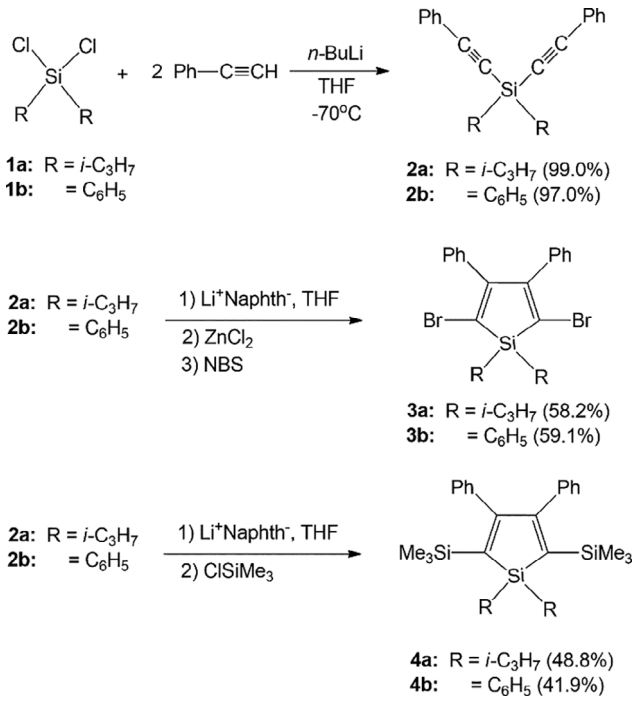

Scheme 1. Synthesis of siloles **3a**, **3b**, **4a**, and **4b**.

Photoelectronic Properties. We studied the photoelectronic properties of the compounds **3a,b** and **4a,b** in THF solution. The spectral characteristics of the silole **3a** have been illustrated in Figure 1 and Table 1. The absorption maximum ($\lambda_{abs,max}$) of **3a**, **3b, 4a**, and **4b** were found at 325, 333, 303, and 311 nm, respectively, with molar absorptivities between 1.85×10^3 and 2.18×10^3 cm^{-1} M^{-1}. These strong absorption bands in the UV–Vis spectra of **3a,b** and **4a,b** might be due to the characteristic chromophore groups of phenyl and diene in the 3,4-diphenyl-siloles.[25] On comparing the absorption maximum ($\lambda_{abs,max}$) of **3a,b** with those of **4a,b** in THF, we observed a bathochromic shift of 22 nm. This shift may be attributed to the strong intramolecular interactions through the electron-rich bromine groups.[25]

Figure 2 depicts the highest occupied molecular orbital (HOMO) and the lowest unoccupied molecular orbital (LUMO) diagrams of **3a**, **4a**, and **4b**, calculated by density functional theory (DFT) using the Gaussian 09 W and B3LYP/6-31G basis set. The HOMO-LUMO band gaps for the siloles **3a**, **4a**, and **4b** (Figure 2) were calculated to be 1.88, 3.32, and 3.27 eV, respectively. The values are in agreement with the absorption maximum ($\lambda_{abs,max}$) in the UV–Vis spectra, attributed to the π-conjugated silole ring.[3]

The excitation peaks of **3a**, **3b**, **4a**, and **4b** collected at 445, 443, 409, and 414 nm were observed at the maximum of the excitation bands ($\lambda_{ex,max}$), 371, 376, 347, and 368 nm, respectively, as illustrated in Figure 1 and Table 1. The emission maximum ($\lambda_{em,max}$) of **3a**, **3b**, **4a**, and **4b** on excitation at 371, 376, 347, and 368 nm, respectively, was observed at 445, 443, 409, and 414 nm, respectively (Figure 1 and Table 1). The intense excitation and emission peaks observed for the prepared siloles **3a,b** and **4a,b** are attributed to the chromophores of the phenyl and diene groups in the 3,4-diphenyl-silole ring.[26] Furthermore, the full width at half maximum (FWHM) of the emission spectra of **3a**, **3b**, **4a**, and **4b** were measured as 83, 71, 99, and 127 nm, respectively, as shown in Table 1.

Cyclic Voltammetric Characteristics. We studied the cyclic voltammetric characteristics of the siloles **3a**,**b** and **4a**,**b** by coating the synthesized siloles on copper electrodes.

The working electrode was fabricated by dipping a copper electrode into a hexane solution of each synthesized silole. The cyclic voltammograms of the siloles **3a** and **4a** on the copper electrode in aqueous sulfuric acid (1.0 M H_2SO_4) and potassium hydroxide solution (1.0 M KOH) are shown in traces (a) and (b), respectively, in Figure 3 and Table 1. The cyclic voltammograms of **3a** and **3b** exhibit a single oxidation peak at 0.90 and 0.80 V, respectively, vs. the reference electrode of Ag/Ag^+. The reduction peak of **3a** and **3b** was observed at −1.20 and −1.20 V, respectively, vs. Ag/Ag^+ electrode. The cyclic voltammograms of **4a** and **4b** show two oxidation peaks at −0.40, −0.05, and −0.55, −0.95 V vs. the Ag/Ag^+ reference electrode. The corresponding two reduction peaks

Table 1. Selected characteristics of silole derivatives **3a**, **3b**, **4a**, and **4b**.

Siloles	^{1}H NMR[a] δ (ppm)	^{13}C NMR[b] δ (ppm)	^{29}Si NMR[c] δ (ppm)	Absorption[d] $\lambda_{abs,\ max}$ (ε) (nm (cm^{-1} M^{-1}))	Excitation[e] $\lambda_{ex,\ max}$ (nm)	Fluorescence[f] $\lambda_{em,\ max}$ (nm)	Fluorescence FWHM[g] (nm)	CV[h]
3a	1.26, 1.52, 6.94, 7.15	9.80, 17.17, 119.77, 127.35, 127.55, 128.96, 137.29, 157.87	7.46	325 (1.91 × 10^3)	371	445	83	Epa +0.90 Epc –1.20
3b	7.02, 7.18, 7.53, 7.86	120.04, 127.60, 127.62, 127.97, 128.51, 129.03, 131.19, 135.78, 136.90, 158.22	–16.49	333 (2.18 × 10^3)	376	443	71	Epa +0.80 Epc –1.20
4a	–0.17, 1.15, 1.44, 6.79, 7.01	1.18, 11.88, 18.42, 125.90, 126.93, 129.19, 140.84, 143.35, 171.93	–9.92, 35.60	303 (1.85 × 10^3)	347	409	99	Epa –0.40, –0.05 Epc –0.55, –0.93
4b	0.00, 7.34, 7.47, 7.86, 8.23	0.70, 126.18, 122.99, 129.73, 132.63, 135.67, 142.61, 143.66, 171.66	–8.86, 8.41	311 (2.12 × 10^3)	368	414	127	Epa –0.55, –0.95 Epc –0.45, –0.10

[a] In $CDCl_3$. [b] In $CDCl_3$. [c] In $CDCl_3$. [d] In THF. [e] Detection wavelengths 445, 443, 409, and 414 nm in THF for **3a**, **3b**, **4a**, and **4b**, respectively. [f] Excitation wavelengths 371, 376, 347, and 368 nm in THF for **3a**, **3b**, **4a**, and **4b**, respectively. [g] FWHM = full width at half maximum. [h] Cyclic voltamogram. Epa = oxidation potential, Epc = reduction potential.

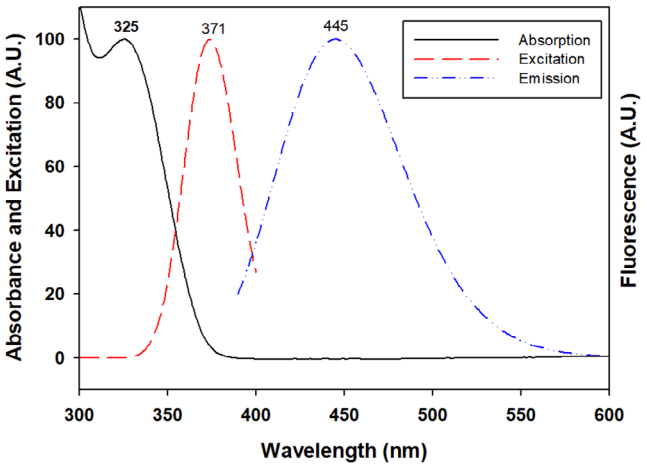

Figure 1. Absorbance, excitation, and emission spectral traces of **3a** in THF solution.

occur at −0.55, −0.93, and −0.45, −0.10 V, respectively. Based on the observations of the electrochemical studies, it can be inferred that the reduction procedures reflect the transformations of **3a,b** and **4a,b** into the equivalent anions of **3a,b** and **4a,b**, for example, $[\mathbf{3a,b}]^-$ and $[\mathbf{4a,b}]^-$ or $[\mathbf{4a,b}]^{-2}$, respectively. The oxidation processes might illustrate the reverse transformations of the equivalent anions of **3a,b** and **4a,b**, for instance, $[\mathbf{3a,b}]^-$ and $[\mathbf{4a,b}]^-$ or $[\mathbf{4a,b}]^{-2}$ into the initial **3a,b** and **4a,b**, respectively.[27–29]

These photoelectronic and cyclic voltammetry properties of the siloles **3a**, **3b**, **4a**, and **4b** indicate that the prepared siloles are potential candidates for electrochemical device applications.

Morphologies of the Electrode Surface. We examined the surface morphologies of the pristine electrode coated with the anode silole material **4a**, using field emission scanning electron microscopy (FE-SEM) with energy-dispersive X-ray spectroscopy (EDXS), as shown in Figure 4(a)–(e).[30,31] Figure 4(a) stipulates that the surface of the pristine

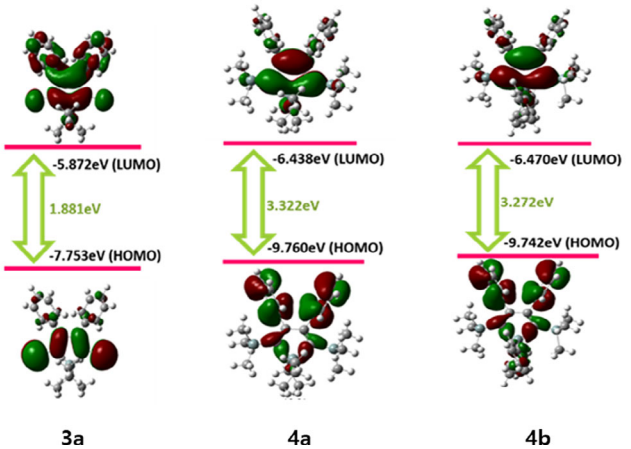

Figure 2. HOMO/LUMO diagrams and energy gaps of **3a**, **4a**, and **4b**.

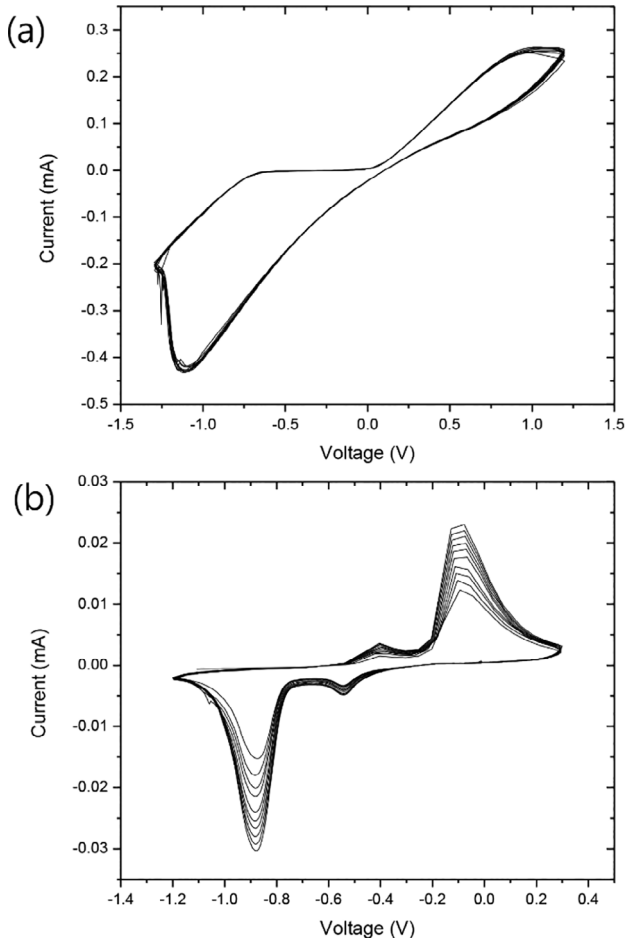

Figure 3. Cyclic votammogram traces of (a) **3a** in an aqueous solution of 1.0 M H_2SO_4 and (b) **4a** in an aqueous solution of 1.0 M KOH.

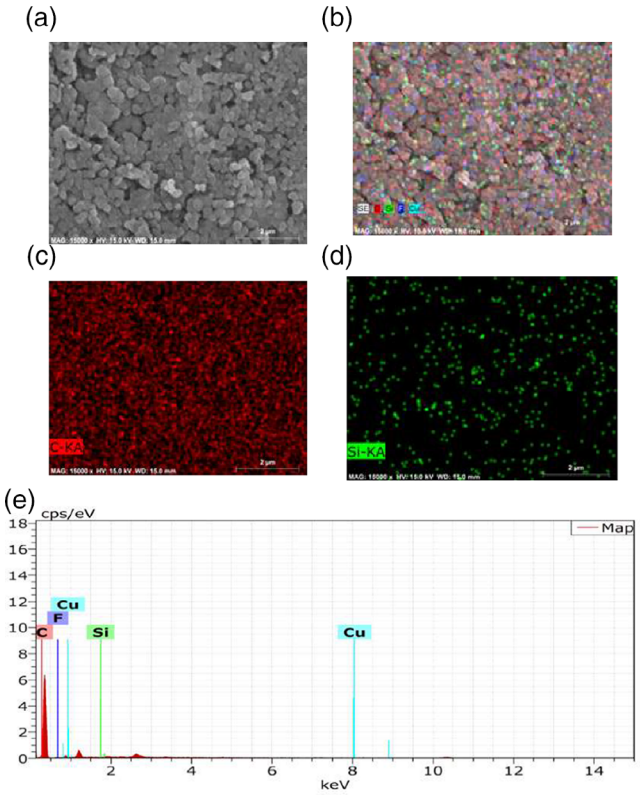

Figure 4. SEM images and EDXS analysis chart of the pristine electrode coated with the anode material **4a**. (a) SEM image of electrode. (b) Component analysis mapping of the electrode. (c) Carbon element-based mapping. (d) Silicon element-based mapping. (e) EDXS analysis chart of the electrode used with the anode material **4a**.

electrode coated with the anode silole **4a** was smooth. Figure 4(b)–(e) indicates that the component elements of silicon and carbon on the pristine cell electrode were well deposited.

Long Cycling Performance Property. We studied the long cycling performance properties of the anode silole materials **3a**, **4a**, and **4b** at a current density of 1 A/g, based on their cyclic voltammogram results, as shown in Figure 5.[32] Compound **4a** exhibits a better long-cycle performance by almost 1000 cycles as compared that of **3a** and **4b**. In the case of **4a**, the first discharge/charge capacities were found to be 973/509 mAh/g with a Coulombic efficiency of 52.3% at 13 cycles. A charge capacity of 708 mAh/g with a Coulombic efficiency of 72.8% was achieved at 200 cycles and 900 mAh/g charge capacity along with a Coulombic efficiency of 92.5%, achieved at 438 cycles. Subsequently, the charge capacities of the anode material **4a** slowly decreased to 762 mAh/g with a Coulombic efficiency of 78.4% after 876 cycles. The value increased slightly to 784 mAh/g with a Coulombic efficiency of 80.6% after 1000 cycles. The gradual increase in the capacity during the cycling process may be a result of the highly reversible lithium ion exchange, as indicated in the cyclic voltammogram of **4a** in Figure 3.[29] The plausible reason for the gradual decrease in the capacity is the

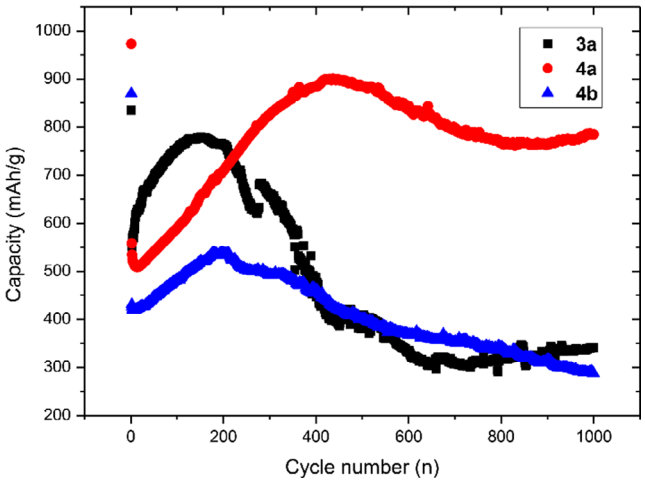

Figure 5. Long cycling performances of the anodes **3a, 4a**, and **4b**.

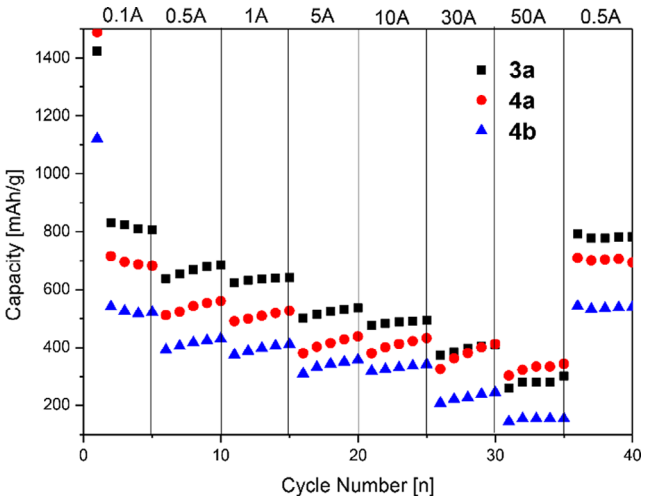

Figure 6. Rate performances of the anodes **3a**, **4a**, **and 4b**.

side reactions of **4a** with the conductor or electrolyte being used.[29]

Rate Performance Property. The battery performances of the silole anodes **3a**, **4a**, and **4b** were illustrated at different C-rates, as shown in Figure 6.[32] In the case of the silole anode **3a**, the cell delivered reversible capacities of 832 mAh/g at 0.1C, 637 mAh/g at 0.5C, 624 mAh/g at 1C, 501 mAh/g at 5C, 476 mAh/g at 10C, and 372 mAh/g at 30C. The cell of **4a** delivered reversible capacities of 716 mAh/g at 0.1C, 511 mAh/g at 0.5C, 490 mAh/g at 1C, 380 mAh/g at 5C, 380 mAh/g at 10C, and 325 mAh/g at 30C. These results show that the Li-**3a** and Li-**4a** cells deliver 44 and 45% of discharge capacities at 30C, respectively, compared to those at 0.1C. Although the cycling at 50C resulted in low discharge capacities of 259 and 412 mAh/g, further cycling at a low rate of 0.5C brought back the capacities to 792 and 709 mAh/g, which correspond to 95 and 99% retention of the initial capacities, respectively. These results indicate that the rate performances of the Li-**3a** and Li-**4a** cells are superior to that of the Li-**4b** cell.

Discharge and Charge Curves and Electrochemical Impedance Spectroscopy. We studied the discharge and charge performance properties as well as the electrochemical impedance spectroscopy (EIS) of **4a**, as shown in Figure 7.[32] Figure 7(a) depicts the discharge and charge curves of **4a** after the 1st to 1000th cycle at a current density of 1 A/g in the range of 0–3 V. It can be seen from Figure 7(a) that the silole **4a** features one plateau at approximately 0.58 V of the first discharge curve and the initial discharge specific capacity of the **4a** electrode is 972 mAh/g. The initial capacity decreased to 520 mAh/g of the discharge specific capacity after the fifth cycle and then increased to 540 mAh/g from the 50th cycle as the cycling proceeds. The value reaches 884 mAh/g with an initial Coulombic efficiency of 91% after the 500th cycle and

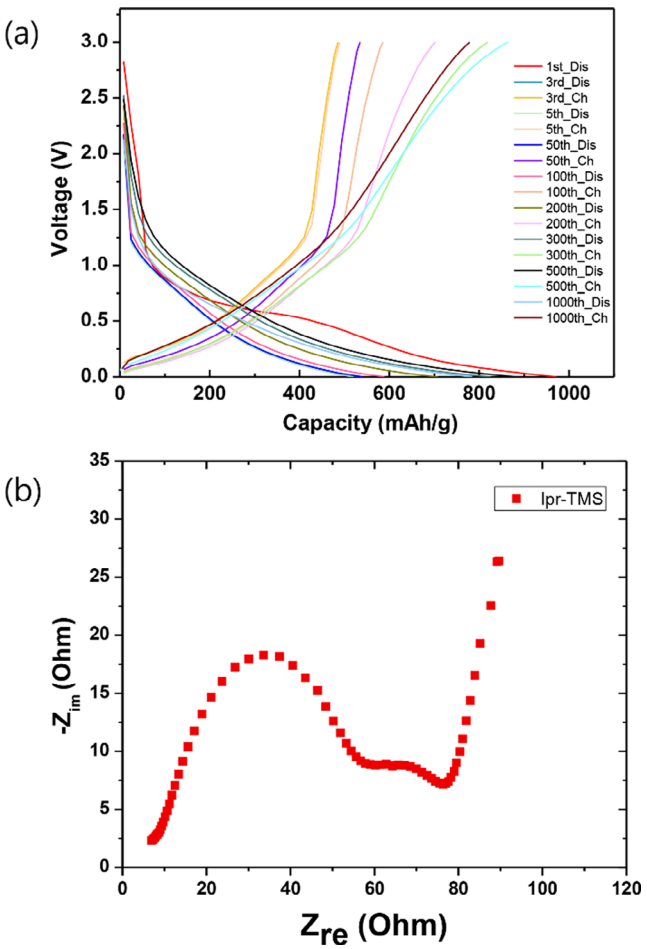

Figure 7. (a) Discharge and charge curves of **4a** in the 1st to 1000th cycle at a constant current density of 1A/g. (b) Electrochemical impedance spectrum of the **4a** after all the discharge–charge test, presented as Nyquist plot.

finally, after the 1000th cycle, the value is 784 mAh/g (initial Coulombic efficiency of 81%).

Figure 7(b) shows the electrochemical impedance spectroscopy (EIS) image of the silole anode material **4a** that is represented as the Nyquist plot obtained using AC electrochemical impedance spectroscopy.[33,34] The EIS measurement was carried out with half cells after all the discharge–charge tests. The plot reveals two partially overlapped semicircles in the frequency range of 100 000 to 0.05 Hz and a straight sloping line at low frequencies. The intercept of the semicircle appearance, 7 Ω, is the bulk resistance (R_b). The first semicircle is correlated with the resistance of the solid-state interface layer (R_{sei}), 57 Ω. The second semicircle is correlated with the charge transfer resistance (R_{ct}) of 76 Ω, indicating the contact resistance between the electrode and electrolyte. The inclined straight line of the plot in the low-frequency region is closer to the vertical line along the imaginary axis, implying low charge transfer resistance and good conductivity of the electrolyte as well as fast chemical adsorption/desorption rate of

electrolyte ions on the electrode surface. This phenomenon may be a result of the partially conjugated electronic structure and the isopropyl side group of the active material (the silole **4a**), as shown in the HOMO/LUMO diagrams and energy gaps in Figure 2.[2,3]

Conclusion

In this work, we report the intramolecular cyclization of 1,1-diisopropyl- or diphenyl-bis(phenylethynyl)-silanes (**2a** and **2b**), followed by the bromination or trimethylsilylation to obtain 1,1-diisopropyl- or -diphenyl-3,4-diphenyl-2,5-dibromo-siloles (**3a** and **3b**) and 1,1-diisoproyl- or -diphenyl-3,4-diphenyl-2,5-bis(trimethylsilyl)-siloles (**4a** and **4b**), respectively. We studied the structures of **3a**,**b** and **4a,b** using ^{1}H, ^{13}C, and ^{29}Si NMR as well as FTIR spectroscopy. The THF solutions of the silole derivatives **3a**,**b** and **4a,b** exhibited absorption bands at 303–325 nm with molar absorptivities of 1.85×10^{3}–2.18×10^{3} $cm^{-1} \cdot M^{-1}$, excitation bands at 347–376 nm, and emission peaks at 409–445 nm. The experimental absorption, excitation, and emission data illustrated that the silole skeleton in all the derivatives comprise chromophores like phenyl and 1,4-diene of 3,4-diphenyl-1-silacyclopenta-2,4-dienylene. The cyclic voltammograms of **3a** and **3b** indicated oxidation peaks at 0.90 and 0.80 V and reduction peaks at −1.20 and − 1.20 V, respectively. However, the cyclic voltammograms of **4a** and **4b** indicated two oxidation peaks between −0.05 and − 0.95 V and two reduction peaks between −0.10 and − 0.93 V, respectively. Compound **4a** exhibits a better long cycle performance by almost 1000 cycles as compared that of **3a** and **4b**. The rate performance test of the anodes **Li-3a** and **Li-4a** indicated better performance properties at various C rates as compared to that of Li-**4b**. According to the discharge–charge curves, **4a** shows one plateau at approximately 0.58 V of the first discharge curve and an initial discharge specific capacity of 972 mAh/g. The electrochemical impedance spectroscopy of **4a** shows a low charge transfer resistance, good conductivity of the electrolyte, and fast chemical adsorption/desorption rate of the electrolyte ions on the electrode surface. These observations can be attributed to the partially conjugated electronic structure and the isopropyl side group of the silole **4a**. The photoelectronic and electrochemical characteristics of **3a**, **4a**, and **4b** imply the potential applications of silole derivatives as novel electronic materials.

Acknowledgment. This research was supported by the National Research Foundation of Korea (NRF), the Ministry of Education of the Republic of Korea (NRF-2020R1I1A3A04036901), and was also supported by Keimyung University.

Supporting Information. Spectrophotometric data of NMR, IR, UV–vis absorption, excitation, and fluorescence emission along with cyclic voltammograms for the compounds **2a,b**, **3a,b**, and **4a,b** are available in the online version of this article.

References

1. (a) E. H. Braye, W. Hübel, *Chem. Ind.* **1959**, 1250. (b) E. H. Braye, W. Hübel, I. Caplier, *J. Am. Chem. Soc.* **1961**, *83*, 4406.
2. J. Dubac, A. Laporterie, G. Manuel, *Chem. Rev.* **1990**, *90*, 215.
3. S. Yamaguchi, K. Tamao, *J. Chem. Soc. Dalton Trans.* **1998**, *22*, 3693.
4. T. Sanji, T. Sakai, C. Kabuto, H. Sakurai, *J. Am. Chem. Soc.* **1998**, *120*, 4552.
5. J. Chen, B. Xu, K. Yang, Y. Cao, H. Sung, I. Williams, B. Tang, *J. Phys. Chem.* **2005**, *109*, 17086.
6. K. Geramita, J. McBee, Y. Shen, N. Radu, T. Tilley, *Chem. Mater.* **2006**, *18*, 3216.
7. C. Ding, G. Babu, A. Orita, T. Hirate, J. Otera, *Synlett* **2007**, *16*, 2559.
8. C. K. W. Jim, R. Hu, M. Faisal, J. W. Y. Lam, B. Z. Tang, *Polym. Prepr. (Am. Chem. Soc., Div. Polym. Chem.)* **2011**, *52*, 842.
9. Y. T. Park, *Bull. Kor. Chem. Soc.* **2016**, *37*, 56.
10. A. J. Boydston, Y. Yin, B. L. Pagenkopf, *J. Am. Chem. Soc.* **2004**, *126*, 10350.
11. K. Tamao, S. Yamaguchi, M. Shiro, *J. Am. Chem. Soc.* **1994**, *116*, 11715.
12. J. Oshita, N. Mimura, H. Arase, M. Nodono, A. Kunai, K. Komaguchi, M. Shiotani, *Macromolecules* **1998**, *31*, 7985.
13. M. S. Liu, J. Luo, A. K.-Y. Jen, *Chem. Mater.* **2003**, *15*, 3496.
14. Z. Liu, J. Zou, J. Chen, Y. Cao, *Polymer Preprints (Am. Chem. Soc., Div. Polym. Chem.)* **2009**, *50*, 485.
15. Z. Zhao, D. Liu, F. Mahtab, L. Xin, Z. Shen, Y. Yu, C. Y. K. Chan, P. Lu, J. W. Y. Lam, H. H. Y. Sung, I. D. Williams, B. Yang, Y. Ma, B. Z. Tang, *Chem. Eur. J.* **2011**, *17*, 5998.
16. H.-J. Son, W.-S. Han, H. Kim, C. Kim, J. Ko, C. Lee, S. O. Kang, *Organometallics* **2006**, *25*, 766.
17. (a) Y. T. Park, *Bull. Kor. Chem. Soc.* **2014**, *35*, 1825. (b) Y. M. Jung, S.-H. Baek, Y. T. Park, *Bull. Kor. Chem. Soc.* **2017**, *38*, 91. (c) J. H. Jang, Y. T. Park, *Bull. Kor. Chem. Soc.* **2018**, *39*, 313. (d) Y. M. Jung, J. H. Jang, Y. T. Park, *Bull. Kor. Chem. Soc.* **2019**, *40*, 192.
18. (a) J. Y. Park, Y. M. Jung, Y. T. Park, *Bull. Kor. Chem. Soc.* **2020**, *41*, 15. (b) Y. T. Park, Y-h. Cho, J. Y. Park, Y. M. Jung, S-H. Baek, Korea Patent 10–2064673, **2020**.
19. W. L. F. Armarego, D. D. Perrin, *Purification of Laboratory Chemicals*, 4th ed., Butterworth-Heinemann, Oxford, **1996**.
20. N. A. Morra, B. L. Pagenkopf, *Org. Synth.* **2008**, *85*, 53.
21. E. Pretsch, P. Bühlmann, C. Affolter, *Structure Determination of Organic Compounds, Tables of Spectral Data*, 3rd ed., Springer-Verlag, Berlin, **2000**.
22. R. M. Silverstein, F. X. Webster, D. J. Kiemle, *Spectrometric Identification of Organic Compounds*, 7th ed., John Wiley & Sons, Hoboken, NJ, **2005**.
23. E. A. Williams, NMR Spectroscopy of Organosilicon Compounds. In *The Chemistry of Organic Silicon Compounds*, Vol. *1*, S. Patai, Z. Rappoport Eds., Wiley, Chichester, UK, **1989** Chapter 8.

24. L. J. Bellamy, *The Infra-Red of Complex Molecules*, 3rd ed., John Wiley and Sons, New York, NY, **1975**.
25. S. Yamaguchi, R.-Z. Jin, Y. Itami, T. Goto, K. Tamao, *J. Am. Chem. Soc.* **1999**, *121*, 10420.
26. N. N. Barashkov, O. A. Gunder, *Fluorescent Polymers*, Ellis Horwood, London, UK, **1994**.
27. H. Maruyama, H. Nakano, M. Nakamoto, A. Sekiguchi, *Angew. Chem.* **2014**, *126*, 1348.
28. Y. Chen, S. Zeng, J. Qian, Y. Wang, Y. Cao, H. Yang, X. Ai, *Appl. Mater. Interfaces* **2014**, *6*, 3508.
29. (a) S. Gottis, A.-L. Barès, F. Dolhem, P. Poizot, *ACS Appl. Mater. Interfaces* **2014**, *6*, 10807. (b) H. H. Lee, Y. Park, K.-H. Shin, K. T. Lee, S. Y. Hong, *ACS Appl. Mater. Interfaces* **2014**, *6*, 19118.
30. J. Lee, H. Kim, M. J. Park, *Chem. Mater.* **2016**, *28*, 2408.
31. (a) T. Zhang, E. Olsson, M. Choolaei, V. Stolojan, C. Feng, H. Wu, S. Wang, Q. Cai, *Materials* **2020**, *13*, 1132. (b) K. S. Kang, M. J. Seong, S. H. Oh, J. -S. Yu, T. Yim, *Bull. Kor. Chem. Soc.* **2020**, *41*, 1107.
32. (a) S. Goriparti, E. Miele, F. D. Angelis, E. D. Fabrizio, R. P. Zaccaria, C. Claudio, *J. Power Sources* **2014**, *257*, 421. (b) J. K. Kang, J. W. Park, J. Kang, J. H. Kang, Y. Jung, *Bull. Kor. Chem. Soc.* **2019**, *40*, 517.
33. (a) B.-L. He, B. Dong, H.-L. Li, *Electrochem. Commun.* **2007**, *9*, 425. (b) M. Sohn, D. G. Lee, D. J. Chung, A. Kim, H. Kim, *Bull. Kor. Chem. Soc.* **2019**, *40*, 150.
34. Z. Lei, Y. X. Yang, S. Guo, W. Sun, H. Liu, L.-P. Lv, Y. Zhang, *Nat. Commun.* **2018**, *9*, 576.

